Investigations of Optical Line Shapes and Kinetic Hole Burning in Myoglobin†

Vukica Šrajer‡ and Paul M. Champion*

Department of Physics, Northeastern University, Boston, Massachusetts 02115

Received February 15, 1991; Revised Manuscript Received April 29, 1991

ABSTRACT: We present the results of an extensive investigation of the optical line shapes of deoxymyoglobin (Mb), the ligand-bound form (MbCO), and the low-temperature photoproduct (Mb*). The thermal properties and the pH dependence of the Soret band and the near infrared band III (~760 nm) are analyzed, taking into account the underlying vibrational properties of the absorption bands. The strong temperature dependence associated with the Soret band of MbCO and band III of Mb indicates significant coupling to low-frequency modes that may not be directly observed in the resonance Raman spectra. On the basis of analogous line-shape studies in a variety of heme systems, we assign the low-frequency coupling in MbCO to torsional motions of the CO molecule. The low-frequency mode coupled to band III (~70 cm^{-1}) is found to lie quite close to the value for the heme-doming motion (~50 cm^{-1}) calculated by using the kinetically determined value of the force constant (17 N/m). Significant inhomogeneous broadening in the Soret region of Mb and Mb* is found to be due to a "nonkinetic" coordinate that we associate with the orientation of the proximal histidine. A "kinetic" coordinate, associated with the equilibrium displacement of the iron atom from the porphyrin plane (a) is found to contribute to the inhomogeneous broadening of both the Soret band and band III. The relaxation of the heme as the system evolves from from Mb* to Mb is followed optically as a function of temperature, and a sharp transition temperature is found at 185 K. The blue shifts of the Soret band and band III as Mb* evolves to Mb are found to be nearly identical ($\Delta\tilde{\nu}^{*}_{ABS} \sim 140$ cm^{-1}) and attributed to changes in the mean value of a between Mb* (a_0^*) and Mb ($a_0 = 0.45$ Å). A simple quadratic model for the coordinate coupling that simultaneously accounts for the observed shift, $\Delta\tilde{\nu}^{*}_{ABS}$, the low-temperature kinetics and the kinetic hole burning predicts $a_0^* = 0.2 \pm 0.05$ Å and $E_A = 16 \pm 2$ kJ/mol for the room temperature Arrhenius barrier height at the heme. A simple quantitative method for the analysis of kinetic hole-burning experiments is also developed and applied to recent studies involving quaternary and subunit-specific hemoglobin structures.

Heme proteins constitute an important class of biomolecules that are involved in a wide variety of fundamental ligand-binding, catalysis, and electron transport reactions. The electronic structure and covalent linkage of the heme prosthetic group, located at the active site of the macromolecule, clearly plays a central role in the biochemical activity and functional diversity of heme proteins. Nevertheless, the interaction between the heme and the protein motions is also of inherent interest, since the fluctuations and conformational changes of the surrounding protein matrix can lead to dynamic modulations of the heme geometry that affect its reactivity.

As a specific example, we consider the binding of diatomic ligands to myoglobin (Mb), where the heme is covalently linked to the protein through a single amino acid (the proximal histidine). Flash photolysis experiments have revealed the existence of protein conformational substates that interconvert on time scales much slower than the ligand recombination times, at temperatures below 180 K (Austin et al. 1975). The strong electron–nuclear coupling, associated with the electronic spin-state change of the heme iron, leads to significant nuclear rearrangement or reorganization (localized at the heme-histidine site) when a diatomic ligand binds to, or dissociates from, the heme. The nuclear coordinate most profoundly affected by the iron electronic state change involves the doming of the heme and the movement of the iron–histidine moiety away from the porphyrin plane. This rearrangement can be quantified by the mean out-of-plane displacement or equilibrium position of the heme iron atom, $\langle a \rangle$. For example, in the CO bound state $\langle a \rangle \sim 0$ and in the "deoxy", or unbound, state $\langle a \rangle \equiv a_0 \sim 0.45$ Å (Kuriyan et al., 1986). Because of this large change in the nuclear coordinates, the relatively weak force constants (K) expected for heme doming motions can lead to a substantial nuclear reorganization (or Stokes shift) energy that must be considered in the analysis of the ligand-binding reaction. For example, if we take $K \sim 15$ N/m ~ 0.15 mdyn/Å (Warshel, 1977; Šrajer et al., 1988), we find that the heme localized reorganization energy is on the order of $^1/_2 K a_0^2 \sim 10$ kJ/mol (2.4 kcal/mol).

Scheme I

$$\mathrm{MbCO} \underset{}{\overset{\gamma}{\rightleftharpoons}} (\mathrm{Mb^*, CO}) \overset{T>185K}{\dashrightarrow} \mathrm{Mb + CO}$$

We have recently (Šrajer et al., 1988) put forward a simple, quantitative, model (SRC) that includes these heme-doming forces and allows for the explicit coupling of the heme coordinate to a generalized protein coordinate. Thus, as the protein undergoes thermally driven conformational fluctuations (or, in the case of Hb, other structural rearrangements), the heme reactivity is modulated via the altered heme geometry. For example, if the protein conformational changes are coupled to the heme in such a way that the out-of-plane equilibrium displacement is changed from 0.45 to 0.35 Å, there will be a difference in the heme-localized reorganization energy (associated with ligand binding) on the order of 1 kcal/mol. In a more general model, which allows changes in the force constant K, even larger heme-localized energies can arise [see

†This work is supported by NIH Grant AM 35090 and NSF Grant DMB8716382.

*To whom correspondence should be addressed.

‡Present address: Department of Biochemistry and Molecular Biology, University of Chicago, Chicago, IL 60637.

0006-2960/91/0430-7390$02.50/0

Appendix in Šrajer et al. (1988)].

A key difference between the SRC model and prior models, AH (Agmon & Hopfield, 1983) and YB (Young & Bowne, 1984), is the explicit separation of the coordinates associated with the heme from those associated with the protein. The earlier models utilize a single generalized protein coordinate (x) that is held constant below a glass transition temperature ($T_f \sim 180$ K). Thus, the previous models describe the low-temperature flash photolysis experiments depicted in Scheme I without any significant heme relaxation or reorganization energy in the transitions between (Mb*, CO) and MbCO [instead, all of the relaxation in the AH model occurs between (Mb*, CO) and Mb + CO]. In contrast, the SRC model allows for energetically significant heme relaxation to a mean out-of-plane displacement, $\langle a \rangle \equiv a_0^*$, in the low-temperature photoproduct (Mb*, CO). A distribution of heme out-of-plane equilibrium positions (and reorganization energies) arises from the different protein conformations that are trapped upon cooling below T_f (quenched disorder), leading to different values of a for each protein conformation.[1] Such a distribution of reorganization energies (and the associated barrier heights) accounts quantitatively (Šrajer et al., 1988) for the nonexponential rebinding of CO to Mb* observed between 60 and 160 K (Austin et al., 1975).

Above $T_f \sim 180$ K, the various distributions must be allowed to evolve with both time and temperature, since the protein and the heme can relax from the photoproduct state (Mb*, CO) to the deoxy state, Mb + CO, as shown in Scheme I. (The dashed lines indicate the possibility of intervening states on the relaxation pathway.) The relaxation process at temperatures above T_f has been treated by using both a "bounded diffusion" model (Agmon & Hopfield, 1983; Agmon, 1988) and a more empirical stretched exponential approach (Steinbach et al., 1991). Some of the experiments presented here demonstrate the diffusion, or relaxation, of the heme as it evolves from Mb* to Mb, by monitoring the optical difference in the Soret region. Use of a new protocol, which involves laser irradiation upon freezing the sample, leads to a clear definition of the "phase-transition" temperature (185K) where heme relaxation from a_0^* to a_0 becomes possible.

The present study focuses on the optical properties of the heme group and assumes that they provide a probe of its local structure and dynamics. We document below the changes in line shape and position of the Soret band (in MbCO, Mb*, and Mb) and the charge transfer band III at ~760 nm (in Mb* and Mb). We report investigations on the effects of temperature and pH and, where possible, develop quantitative models to account for sources of homogeneous, inhomogeneous, and vibronic broadening. We also utilize the results of recent dynamic studies (Sassaroli & Rousseau, 1987) and kinetic hole-burning experiments (Campbell et al., 1987; Steinbach et al., 1991) to expose and separate the contributions of "kinetic" and "nonkinetic" coordinates to the inhomogeneous broadening of the Soret and 760-nm bands.

Of particular interest is the fact that both the Soret and 760-nm bands of Mb* are red-shifted by ~140 cm^{-1} when compared to Mb. This suggests that both electronic transitions are sensitive to a common coordinate that is altered as Mb* evolves to Mb. If this coordinate is taken to be the "kinetic" coordinate and assigned to the iron out-of-plane displacement, the small kinetic hole burning observed in the Soret transition indicates that additional "nonkinetic" coordinates must be involved in the inhomogeneous broadening of the deoxy Mb and Mb* Soret bands.

In contrast to the Soret band, the 760-nm band reveals only a small amount of inhomogeneous broadening that must be due almost exclusively to the kinetic coordinate. When the thermal dependence of the 760-nm band is analyzed, it is found that a large fraction of the broadening of this band is due to vibronic coupling to low-frequency modes at ~220 cm^{-1}, ~150 cm^{-1}, and below.

A self-consistent analysis of all the optical line shapes, the optical shifts between Mb and Mb*, the low-temperature kinetics, and the kinetic hole burning is presented. Models that utilize both linear and quadratic mapping between the kinetic coordinate and the energy spaces (e.g., optical frequency and barrier height) are compared, with the quadratic model proving superior in its ability to describe the observed line shapes and kinetics.

Finally, we derive closed form expressions that are useful in the quantitative interpretation of kinetic hole-burning experiments. These expressions apply to commonly used kinetic hole-burning protocols that monitor the shift of an optical line shape as a function of rebinding. They also show how such experiments are often insensitive to the magnitude of the coupling between the kinetic coordinate and the barrier height for the reaction.

Experimental Procedures

Lyophilized sperm whale metMb, obtained from Sigma Chemical Co. and United States Biochemical Corp., was used without further purification. For all absorption spectra measurements, the protein was dissolved in an aqueous buffer/glycerol mixture (75% glycerol by volume). For pH 7 samples, 0.1 M potassium phosphate buffer was used, while for lower pH, 0.1 M sodium acetate buffer was used. For deoxy-Mb samples, the solution was equilibrated with N_2 for 1–2 h, and the sample was reduced with an excess of sodium dithionite (in N_2-equilibrated water). For MbCO samples, the solution was equilibrated with 1 atm CO for 1–2 h, reduced with sodium dithionite, and equilibrated again with CO. Typical protein concentrations used were ~10 μM for optical absorption measurements of the Soret band region of Mb and MbCO and ~3 mM for the 760-nm band region of Mb and Mb*.

The samples were placed in a low-temperature transmission cell with two 1.5-mm thick quartz windows. The cell was mounted to the cold finger of an CTI Cryogenics model 22C closed cycle refrigerator, assuring a good thermal contact with an indium gasket. The temperature was regulated with a TRI Research T-2000 Cryo Controller unit and monitored with a cryo-diode mounted on the cold finger. The sample was allowed to equilibrate ~20 min at each temperature.

The absorption spectra were collected with a Perkin-Elmer UV–visible spectrophotometer (model 320) for the deoxy-Mb and MbCO samples. Photolysis of MbCO at 10 K was accomplished by using the strong white light from a quartzline GE 100 W lamp, filtered through a 10-cm water filter. The absorption spectra of Mb* were collected by utilizing the same source and a Spex single monochromator with a 300 g/mm grating and an optical multichannel analyzer (from Princeton Instruments).

Laser light from an argon ion pumped CW dye laser (425 nm), was used in the experiment involving the cooling of the

[1] Note that the protein coordinate x is coupled to a, the equilibrium position of the heme coordinate, *not* to the heme coordinate, Q, itself. Thus, the introduction of the coordinate Q through the heme potential, $(1/2)k(Q-a)^2$, is not a simple replacement of one coordinate by another within the AH model. It can be seen that the two coordinates are not directly correlated, since the heme coordinate, Q, is free to vary at low temperature when x is held constant, i.e., $\partial H(Q,a)/\partial Q|_{Q^*} = 0$ defines the transition state [see eqs 23 and 24 of Šrajer et al. (1988) for details].

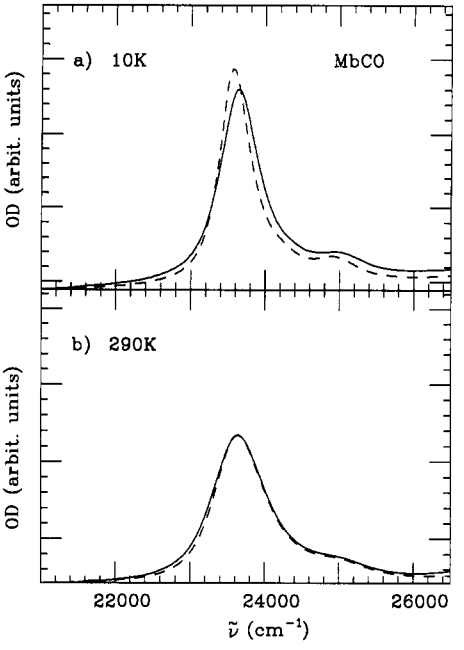

FIGURE 1: MbCO Soret band narrowing at low T. Line shapes at 10 and 290 K are presented for pH 7.3 (75% glycerol) by solid lines and for pH 4.7 (75% glycerol) by dashed lines. The line-shape fits, obtained by the time correlator method (Šrajer et al., 1986), lead to coupling of low-frequency bath modes; $\tilde{\nu}_b S_b \sim 90$ cm^{-1} for pH 7 and ~ 110 cm^{-1} for pH 4.7.

Table I: Temperature Dependence of the Soret Band Line Width

species	δw^a	species	δw^a
CytC, pH 7	0.06	MbCO, pH 7.3 + SO_4^{2-}	0.39
CM-CytC-CO, pH 7	0.22	MbO_2, pH 7.3	0.07
MbCO, pH 7.3	0.26	P450-CO, pH 7	0.23
MbCO, pH 4.7	0.37	$P450_{cam}$-CO, pH 7	0.22

$^a w$ = full width of Soret band at half-maximum (FWHM), $\delta w = [w(290\text{ K}) - w(10\text{ K})]/w(290\text{ K})$.

MbCO sample under illumination. Typical laser power at the sample was ~30 mW. Absorption at 10 K was then monitored by white light. To assure that monitoring was done on the same previously illuminated part of the sample, both light beams (laser and white light) were aligned to pass through and fill two pinholes (0.5-mm diameter) before and after the sample.

Results

MbCO. In Figure 1, we display the Soret band line shapes of MbCO as a function of temperature and pH. The samples are prepared in 75% glycerol, pH 7.3 (solid line) and pH 4.7 (dashed line). The dramatic narrowing of the low-temperature line width in MbCO has been reported previously for samples at pH 7.0 containing 1.0 M ammonium sulfate (Šrajer et al., 1986). The high ionic strength associated with the previous samples leads to spectra that are similar to the low-pH data shown in Figure 1. The spectra taken at 290 K show a small blue shift (~20 cm^{-1}) and slight narrowing of the Soret band when the sample is converted to the A_0 species at low pH [see also Morikis et al. (1991)]. In contrast, the spectra taken at 10 K display a red shift at low pH that is much more prominent (~75 cm^{-1}).

Analogous experiments on other heme systems lead to the results in Table I where we present the line-width changes in the Soret spectra between 290 and 10 K and calculate the percentage decrease in the full width at half-maximum (FWHM). The dramatic difference between the Soret band narrowing of cytochrome c and carboxymethylated (CM)

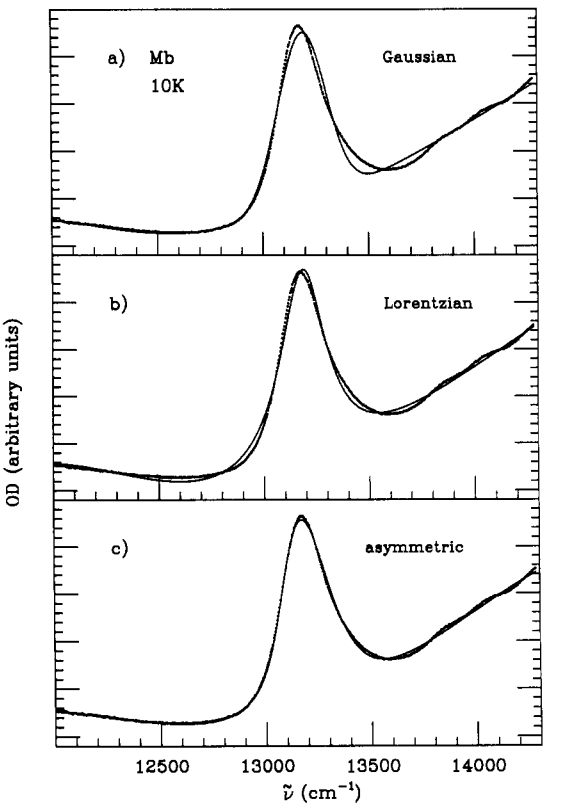

FIGURE 2: Asymmetric line shape of the Mb 760-nm band at 10 K. The attempt to fit this band with a Gaussian line shape ($\sigma_{\tilde{\nu}_0} = 114$ cm^{-1}, $\chi^2 = 6.6 \times 10^{-4}$) is presented in panel a and with a Lorentzian line shape ($\Gamma/2 = 137$ cm^{-1}, $\chi^2 = 4.9 \times 10^{-4}$) in panel b. A convolution of a Lorentzian and a Gaussian (not shown) gives a similar quality fit ($\Gamma/2 = 100$ cm^{-1}, $\sigma_{\tilde{\nu}_0} = 60$ cm^{-1}, $\chi^2 = 4.7 \times 10^{-4}$). A significantly better fit is achieved when the convolution of an asymmetric inhomogeneous broadening ($\sigma_{\tilde{\nu}_0} = 86$ cm^{-1}) and a Lorentzian ($\Gamma/2 = 76$ cm^{-1}) line shape is used ($\chi^2 = 8.8 \times 10^{-5}$), as presented in panel c. Here $\sigma_{\tilde{\nu}_0} \equiv 2\beta_r a_0 \sigma_a$ [see Šrajer et al. (1986) and eqs 3-5]. In all cases a background is added that consists of a constant offset and two Gaussians at ~11 800 and ~15 000 cm^{-1}. The background is adjusted in each case in order to achieve a best fit.

cytochrome c-CO suggests that torsions of the CO rather than librations of the heme are primarily responsible for the thermal "bath" that is coupled to the Soret transition of MbCO.

Deoxy-Mb. The optical spectra of deoxy-Mb are likely to contain information pertaining to heme inhomogeneity, since both the Soret band and band III are expected to respond to the disorder in the iron out-of-plane displacement that occurs in this more "loosely" bound pentacoordinate state. First, we focus on the near infrared band III at 760 nm and illustrate in Figure 2 some quantitative attempts to fit the band by using different functional forms for the line shape. The experimental spectrum is recorded at 10 K and is shown as dotted lines. A least-squares fitting routine, based on the Marquardt algorithm (Bevington, 1986), is used to adjust a background consisting of a constant offset and two Gaussians at ~11 800 and ~15 000 cm^{-1} [see Cupane et al. (1988) for a general discussion of the full range of Mb transitions in the near infrared]. The 760-nm band (~13 200 cm^{-1}) is fit with a Gaussian (a), a Lorentzian (b), and the asymmetric line shape (c) used earlier to describe the inhomogeneous broadening of the deoxy-Mb Soret band (Šrajer et al., 1986). The distinct asymmetry of the band III line shape is not well fit by the symmetric Gaussian or Lorentzian line shapes or by their convolution (Voigt profile). The parameter values associated with the fits in Figure 2 are given in figure caption, where it should be noted that some Lorentzian broadening has also been included in

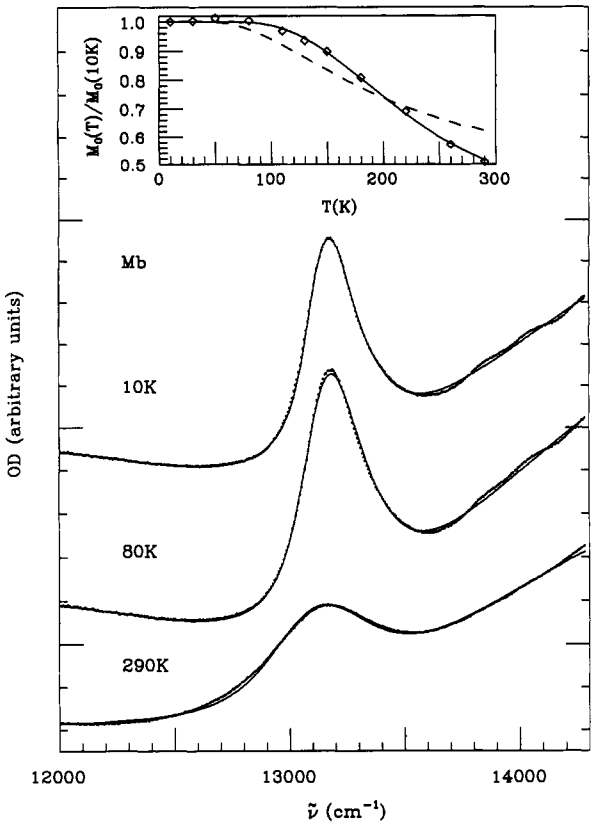

FIGURE 3: Temperature dependence of the Mb 760-nm band. A simultaneous fit to the 10, 80, and 290 K data is shown as solid lines. In order to account for the line-shape narrowing, a low-frequency bath mode (69 cm^{-1}) and two low-frequency modes (150 and 220 cm^{-1} are assumed to be coupled to this transition. The best simultaneous line-shape fits are then achieved with $S_{69} = 0.8$, $S_{150} = 0.023$, $S_{220} = 0.08$, and $\Gamma/2 = 77.4$ cm^{-1} ($\chi^2 = 6.4 \times 10^{-5}$). A small amount of asymmetric inhomogeneous broadening, as in Figure 2 ($\sigma_{\tilde{\nu}_0} = 26$ cm^{-1}) is also found to contribute to the line shape (if a Gaussian inhomogeneous broadening is used $\chi^2 = 9.0 \times 10^{-5}$, $\sigma_{\tilde{\nu}_0} = 24$ cm^{-1}, while the absence of inhomogeneous broadening leads to $\chi^2 = 7.0 \times 10^{-5}$). The insert presents the change in intensity (integrated area, M_0) of the 760-nm band with temperature (diamonds). The attempt to account for the intensity change by a thermal depopulation of the ground state is given as a dashed line for a three-state model with two nearly degenerate states at $\Delta_1 = 241.3$ cm^{-1} and $\Delta_2 = 240.3$ cm^{-1}. The solid line presents an approximation to a multiple excited-state model with nine degenerate states and a single energy gap ($\Delta = 452.8$ cm^{-1}).

panel c to simulate the homogeneous (lifetime) component of the line shape.

The distinct asymmetry of band III at 10 K is also quite evident when the line shape is monitored as a function of temperature, as shown in Figure 3. Note that the simple static distribution functions from the previous figure cannot account simultaneously for both the asymmetric line shape at 10 K and the more Gaussian line shape at 290 K. The most obvious explanation for this type of behavior involves the participation of low-frequency vibrational modes coupled to the electronic excitation associated with band III. However, the usual semiclassical approximation that leads to temperature-dependent Gaussian line shapes, does not sufficiently describe the asymmetry of the band III spectra at low temperatures. As a result, the full quantum mechanical time correlator treatment is needed (Chan & Page, 1984; Šrajer et al., 1986; Schomacker & Champion, 1986). When this treatment is implemented, the fits shown in Figure 3 result.

Notice that the fit to the spectrum at 290 K is still not perfect. This may be due to the choice of mode frequencies, which cannot be determined without independent Raman measurements in resonance with the 760-nm band. In the fits shown in Figure 3, we used modes fixed at 220 and 150 cm^{-1} to simulate the frequencies observed with Soret excitation. The average frequency of the low frequency "bath", $\tilde{\nu}_b$, was determined to be $\sim$70 cm^{-1} by least-squares fitting to the spectra at all temperatures. The coupling strengths were also determined by the least-squares fitting ($S_{220} = 0.08$, $S_{150} = 0.023$, and $S_{70} = 0.8$) and are surprisingly similar to the values found for Soret band excitation (Bangcharoenpaurpong et al., 1984; Šrajer et al., 1986). It should be noted that the spectra could not be fit satisfactorily with only a single low-frequency bath mode.

If temperature-independent[2] inhomogeneous broadening is also allowed, only a small amount ($\sim$25 cm^{-1}) is permitted by the least-squares fitting routine. The caption lists the best-fit parameters for the asymmetric inhomogeneous broadening function used in Figure 3. A Gaussian inhomogeneous distribution with a width of $\sim$25 cm^{-1} would work nearly as well, since most of the asymmetry in the low-temperature line shape is carried by the coupling to the low-frequency subspace.

The insert in Figure 3 shows the normalized intensity of the band III transition as a function of temperature. Since the time correlator analysis does not consider temperature-dependent changes in the oscillator strength, this effect is added separately. The change in the observed intensity is unusually large (nearly a factor of 2 between 10 and 290 K) and cannot be ascribed to the smaller ($\lesssim$10%) solvent contraction effects observed previously for cytochrome *c* (Schomacker & Champion, 1986). However, the possibility of temperature-dependent heme structural changes, induced by solvent contraction in Mb (Cupane et al., 1988), cannot be completely excluded. The theoretical curves, shown in the insert, are based on a simple model that assumes a static heme structure and thermally populated d-orbital electronic states. If excited d-electron configurations of the iron atom are assumed not to contribute to the oscillator strength of band III, the absorption intensity scales with the ground-state population. The dashed line results when only the three lowest orbital states are considered and uses two energy gaps as the fitting parameters. An alternative approach allows for more thermally accessible excited states. For example, use of only a single energy gap that corresponds to an average excited-state energy ($\Delta = 480$ cm^{-1}) and a degeneracy factor ($g = 9$) that is a measure of the number of thermally accessible states leads to much better agreement with the data (solid line).

In Figure 4 we display the Soret band line shapes of deoxy-Mb (pH 7.0) at high and low temperature. The fitting procedure for the high-temperature line shape has been described previously (Šrajer et al., 1986). In order to achieve a satisfactory fit, a significant amount of asymmetric inhomogeneous broadening must be invoked. Strongly coupled low-frequency modes cannot be used to broaden the Soret band line shape, since dramatic narrowing of the Soret band at low temperature is not observed. As previously suggested, the disordered coordinates influencing the Soret transition are likely to involve the iron out-of-plane displacement as well as the tilt and rotation of the proximal histidine with respect to

[2] In general, the inhomogeneous broadening can arise from sources having temperature-dependent modulation amplitudes that add a temperature dependence to the "static" inhomogeneous width above T_f. These thermal effects are proportional to $\sqrt{T/T_f}$ and are usually quite small (<20% of the static inhomogeneous component of the line shape). In the present treatment they are absorbed into the low-frequency "bath" of the time correlator.

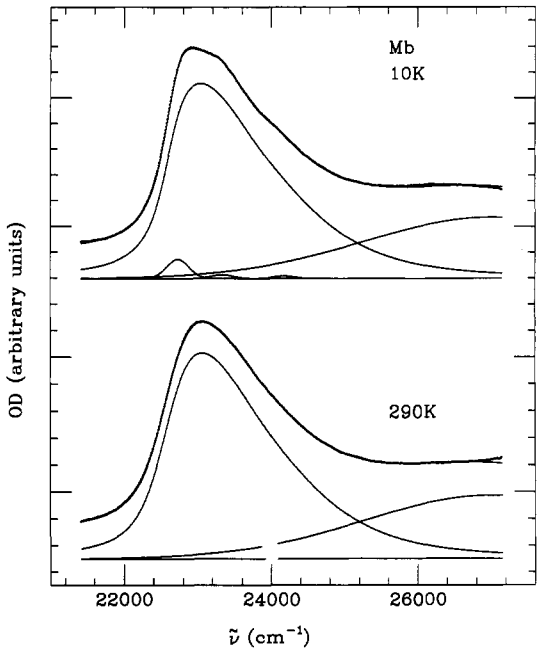

FIGURE 4: Simultaneous fit of the Mb Soret band region at 10 and 290 K. The Mb line shape at both 10 K and room temperature is accounted for by asymmetric inhomogeneous broadening, assuming a Gaussian distribution of a nonkinetic heme coordinate, ϕ, quadratically coupled to the optical transition (see eqs 2–5). Parameters extracted from the fit are $\phi_0/\sigma_\phi = 1.93$ and $\sigma_\phi^2\delta_b = 165.1$ cm^{-1}, which correspond to >500 cm^{-1} of inhomogeneous broadening (eq 6b). A small low-frequency bath was also needed to account for the sharpening of the red edge of the band, $\tilde{\nu}_b S_b = 62$ cm^{-1}. Other parameters are $\Gamma/2 = 243.6$ cm^{-1}, $\tilde{\nu}_{00}$ (10 K) = 22 592.2 cm^{-1}, $\tilde{\nu}_{00}$ (290 K) = 22 567.3 cm^{-1}, and M_0 (10 K)/M_0 (290 K) ~ 0.96. A linear background and a Gaussian at 27 013 cm^{-1} with $\sigma_N = 1739.5$ cm^{-1}, to simulate the N-band, are also allowed to vary with temperature. The weak underlying features observed at 10 K are modeled as Gaussians at 22 735, 22 336, and 24 172 cm^{-1}, with half-widths $\sigma = 150$ cm^{-1}. The fits and the data are overlayed, and the decomposition into components is displaced below.

the heme (Šrajer et al., 1986). In addition to the inhomogeneous broadening, we have used a simple Gaussian in Figure 4 to mimic the blue-shifted transition (N-band) at ~27 000 cm^{-1}. The individual bands and the fit to the full line shape (overlapped with the data) are shown in the figure. At low temperature, there are distinct and reproducible features that grow into the spectrum. These have been modeled as Gaussians with temperature-dependent intensities.

*Low-Temperature Photoproduct Mb**. Figure 5 presents a comparison between the optical transitions of Mb and Mb* at 10 K in 75% glycerol. The distinct red shift of the Mb* transitions (dashed lines) with respect to Mb (solid lines) at pH 7.3 is found to be 2.6 nm for the Soret band and 8 nm for band III. It is important to note that when the shifts of the optical transitions, $\Delta\tilde{\nu}^*_{ABS}$, are converted to energy, we find $\Delta\tilde{\nu}^*_{760} = \Delta\tilde{\nu}^*_{435} = 137$ cm^{-1}.

The red shift of band III by 8 nm in Mb* has been reported earlier (Fiamingo et al., 1985), although other values for the shift of band III have been quoted [e.g., 14 nm, Iizuka et al. (1974)]. We also note that lowering the pH to 4.7, to create more of the "open pocket" species (Morikis et al., 1989), leads to a further shift of band III by ~1.5 nm (dotted line). This effect is too small to be observed in the Soret band due to the compression of the energy scale and loss of resolution in the blue. Since the 760-nm optical transition is presumably much more sensitive to the heme–proximal histidine linkage than to the distal pocket structure, the pH effect suggests that there is some degree of correlation between the distal and proximal conformational changes.

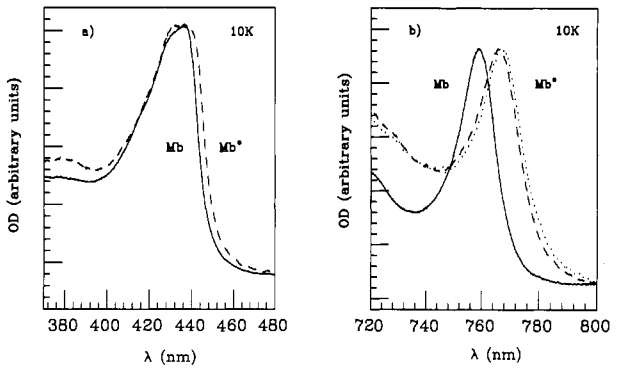

FIGURE 5: Soret and 760-nm bands for Mb (solid lines) and Mb* (dashed lines) at 10 K, pH 7.3 (75% glycerol). In both cases the Mb* band is shifted to the red with respect to Mb band: ~2.6 nm for Soret band and ~8 nm for 760-nm band. The 760-nm band for a pH 4.7 sample of Mb* is shifted to the red from the pH 7.3 band by ~1.5 nm (dotted line). The Soret band does not shift outside the experimental resolution (~20 cm^{-1} = 0.4 nm).

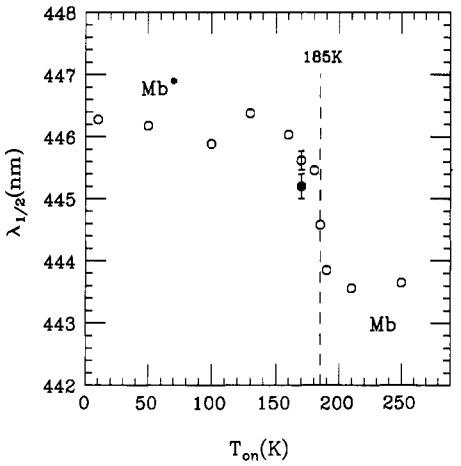

FIGURE 6: Example of using the shift of the Soret band as a probe of the heme relaxation. We plot the red edge position for the Mb* Soret band (at its half-maximum) at 10 K as a function of T_{on} (open circles). A sharp transition at ~185 K between Mb* (446.3 nm) and Mb (443.6 nm) indicates that heme relaxation proceeds on a rapid time scale above this temperature. The solid data point represents an experiment where the sample was kept under illumination at 170 K for 2 h before further cooling.

It is worth noting that the overall line widths of the Mb* transitions are slightly larger (~10%) than for Mb. The larger line widths may be signaling a broader underlying coordinate distribution in Mb*.

In Figure 6 we utilize the shift in the Soret band optical transition to probe a "glass" transition in the MbCO system. We initially begin cooling the sample in the dark, but when the sample temperature reaches T_{on}, it is irradiated through a pinhole with a 425-nm laser beam (~0.05 cm in diameter) until the sample temperature reaches 10 K, whereupon the Soret band is monitored with a strong white light source. The large photon flux associated with the laser light maintains a photodissociated state, and this allows the system to relax from Mb* to Mb during the cooling process from T_{on} to 10 K. The relaxation can involve both the escape of the CO ligand from the heme pocket as well as the doming of the heme from the less out-of-plane position, associated with Mb*, to the fully relaxed position ($a_0 = 0.45$ Å), associated with Mb. Since the optical transition probes this latter process directly, we plot the position of the red edge of the Soret band as determined by its wavelength at half-height ($\lambda_{1/2}$) at 10 K vs T_{on} in order to monitor the onset of heme relaxation. As can be seen from

Table II: Selected Models of the Optical and Kinetic Properties of Mb*[a]

	kinetics		optical					
case	α_H	β_H	α_ν	β_ν	a_0	a_0^*	σ_a	E_A
I	0	51.5	0	781	0.45	0.16	0.1	18
II	0	81	313	0	0.45	0.02	0.08	31
III[b]	37.5	0	241	0	0.62	0	0.1	33
IV[c]	0	25			0.45	0.45	0.15	10

[a] Units for various parameters in this table are α_H (kJ/mol Å), β_H (kJ/mol Å^2), α_ν (cm^{-1}/Å), β_ν (cm^{-1}/Å^2), E_A (kJ/mol). Parameters a_0, a_0^*, and σ_a are in Å. Useful conversions are kcal/mol = 4.18 kJ/mol, N/m = 1.44 kcal/mol Å^2, and kJ/mol = 83.7 cm^{-1}. [b] Case III sets $a_0^* = 0$ and allows no heme relaxation or reorganization on the rebinding trajectory. In this respect a can no longer be identified with the equilibrium position of a coordinate that is free to vary at the barrier crossing. Instead, it is identified with the generalized protein coordinate x and is held constant on the rebinding trajectory for each member of the ensemble. An independent determination of a_0 and σ_a can not be made in case III, since only the ratio a_0/σ_a can be found from fits to the low-temperature kinetics in this model. The arbitrary choice used here follows that of Agmon and Hopfield (1983). [c] The optical parameters in case IV cannot be found because full relaxation leads to $\Delta\tilde{\nu}_{ABS}^* = 0$, which is incompatible with the experimental observation.

the figure, the heme undergoes relaxation from Mb* to Mb on the experimental time scale ($\sim 10^3$ s) when T_{on} is above 185 K but remains in the Mb* state at lower temperatures.

It should be noted that the "amount" of heme relaxation is roughly proportional to both the rate of relaxation (which is primarily determined by the "rigidity" of the glass and T_f) and the time during which relaxation can occur. In the temperature range just below 180 K, where the ligand cannot escape from the heme pocket and the geminate rebinding is comparable to the photolysis rate, the time spent in the photolyzed state, t_{off}, is reduced. Thus, the time during which heme relaxation from Mb* to Mb can occur is also reduced unless extended illumination protocols are employed. In order to test for this effect, the sample was illuminated for $\sim$120 min at 170 K, before further cooling. The result is plotted as the solid data point in Figure 6 and indicates that some photolysis-induced or very slow relaxation toward the Mb state can take place even at this temperature. It has been shown earlier (Šrajer et al., 1991) that extended sample illumination leads to an increased population of molecules for which CO escapes into the cavities of the protein matrix. This results in much slower rebinding rates for these molecules and extends the time scales over which heme relaxation can occur at these higher temperatures.

Discussion and Analysis

MbCO. As discussed in detail previously (Šrajer et al., 1986), we find that, in addition to the resonance Raman active heme modes, the Soret band of MbCO is coupled to a bath of low-frequency modes that are associated with either torsions of the bound CO molecule or librations of the heme (bulk protein modes are unlikely to couple to the localized $\pi \rightarrow \pi^*$ excitation of the heme). Further studies of other heme proteins ligated by diatomic molecules (Table I; Šrajer, 1991) support the role of the diatomic torsions, rather than the heme librations, in the thermal broadening. This is particularly evident from the sharp contrast between the low-temperature narrowing of CO bound CM–cytochrome *c* and native cytochrome *c*, where in both cases the heme is restrained by covalent linkages to the protein. Since the same protein is involved, and the heme librations are presumably reduced by the covalent linkage, we suggest that diatomic torsional motions play a major role in the thermal broadening of the Soret band. The small value of the line width change in MbO_2 may reflect torsional constraints associated with the hydrogen bonding between the distal histidine and the bound oxygen.

As shown earlier with infrared spectroscopy (Shimada & Caughey, 1982; Ansari et al., 1987), there are three major MbCO conformational states known as A_0, A_1, and A_3. These conformations have been assigned (Morikis et al., 1989) to a closed heme pocket (A_1 and A_3) or an open heme pocket (A_0), on the basis of extensive Raman and infrared studies involving pH, ionic strength, and site-directed mutagenesis. The relative populations of the open and closed states depend on the pH and solvent composition and vary with temperature (Hong et al., 1990; Ansari et al., 1987). At pH 7 the closed pocket states dominate and only $\sim$3% of the population is due to A_0 at room temperature (Morikis et al., 1989; Shimada & Caughy, 1982). Since the pocket opens as the pH is lowered, we conclude from Table I that more thermal broadening is present when the pocket is open and the FeCO moiety is less constrained. The temperature dependence of the Raman line shapes of the FeCO and heme modes is consistent with this conclusion (Morikis et al., 1989). Evidently the larger pocket and more upright FeCO bond in the "open" state allow more coupling to the torsional degrees of freedom in this system.

The small shift in Soret band line position with pH in the room temperature samples probably reflects alterations in the FeCO geometry (Ormos et al., 1988; Moore et al., 1988) that are associated with different populations of A states. The much larger changes in the Soret band position at low temperature, and the opposite direction of the shift, are difficult to explain. If FeCO structural differences are responsible, we might expect to observe differences between the low-temperature (Ormos et al., 1988) and room temperature (Moore et al., 1988) geometries of the A_0 state, which is populated at low pH.

Deoxy-Mb. The optical transitions of deoxy-Mb also show significant coupling to low-frequency modes. In particular, the band at 760 nm shows a surprising amount of temperature-dependent asymmetry that cannot be assigned to static inhomogeneous broadening. As will be seen below, the relatively small inhomogeneous broadening allowed by the fits to the data is just the amount needed to quantitatively account for the kinetic hole-burning experiments. Thus, it seems that the observed inhomogeneity in band III is entirely due to a "kinetic coordinate".

The strongly coupled ($S_b = 0.8$) low-frequency mode at $\tilde{\nu}_b \sim 70$ cm^{-1}, needed to account for the thermal properties of the band III line shape, can be tentatively assigned to heme-doming motions. For example, if we estimate the reduced mass of the histidine/iron-porphyrin oscillator as $\sim 1.9 \times 10^{-25}$ kg and use the force constant $K = 17$ N/m (case I, Table II), we find a frequency of 50 cm^{-1}. This is quite close to the frequency needed to explain the temperature dependence of band III.

The temperature dependence of the 760-nm band intensity is quite unusual and suggests the presence of numerous ($g = 9$) low lying excited electronic states in the deoxy-Mb system. This is consistent with several previous studies of the electronic structure of the iron atom in deoxy-Mb that have concluded that additional low lying states, outside the ^{5}D term, are needed

to account for the temperature dependence of Mössbauer quadrupole splitting (Huynh et al., 1974; Kent et al., 1979). Still more sophisticated models could include the possibility of changes in the vibrational frequencies of the heme–histidine system upon d-orbital electronic excitation. This would alter the vibrational energy level density associated with each electronic state and affect the temperature dependence of the electronic state Boltzmann populations.

In contrast to band III, the Soret band line shape is described by a significantly larger amount of inhomogeneous broadening ($\gtrsim$500 cm^{-1}). Thus, as proposed previously (Šrajer et al., 1986), it seems that several disordered coordinates participate in the inhomogeneous broadening of the deoxy-Mb Soret band. The smaller relative contribution of the "kinetic coordinate" (which we take to be the iron out-of-plane displacement in the following discussion), along with the compression of the energy scale in the blue, makes kinetic hole burning much more difficult to quantify in the Soret region. Nevertheless, small effects ($\lesssim$45 cm^{-1}) on the same order as observed for band III have been reported (M. Chance, private communication; Šrajer, 1991).

Thermal-broadening effects are also observed in the deoxy-Mb Soret band and lead to a sharpening of the red edge at low temperature (Figure 4). The magnitude of this effect is quite similar to that observed for the 760-nm band and is characterized by $\tilde{\nu}_b S_b$ = 62 cm^{-1}. As suggested for the 760-nm band, we attribute the low-frequency coupling to doming motions that arise from the flexibility of the pentacoordinate high-spin heme. The absence of such low-frequency coupling in low-spin hexacoordinate compounds, such as cytochrome *c*, supports this suggestion (Schomacker & Champion, 1986).

These transitions have an oscillator strength and temperature-dependent behavior similar to that of the 760-nm band. They probably involve the iron d-orbitals, and their presence in the Soret region may account for the unusually rapid electronic state decay times associated with the Soret band in heme systems.

We also note that the small temperature-dependent features underlying the low-temperature Soret band of deoxy-Mb (Figure 4) are not unprecedented for heme proteins and were observed and documented in detail in an earlier investigation of cytochrome *c* (Schomacker & Champion, 1986). These transitions have an oscillator strength and temperature-dependent behavior similar to that of the 760-nm band. They probably involve the iron d-orbitals and their presence in the Soret region may account for the unusually rapid electronic state decay times associated with the Soret band in heme systems. It is unlikely that the "structure" near the peak of the low-temperature Soret band is due to resolution of the near *x*–*y* degeneracy associated with the heme group. Dispersion of the resonance Raman depolarization ratios is quite sensitive to the *x*–*y* splitting (Collins et al., 1976) but such effects are not observed in the Soret band of deoxy-Mb (Bangcharoenpaurpong et al., 1984).

Given the open shell nature of the high-spin ferrous iron atom, one should also consider the possibility that the entire asymmetry of the line shape might be ascribed to numerous underlying electronic transitions. However, it seems unlikely that there is enough oscillator strength associated with these transitions to account for the overall asymmetry of the Soret band line shape without severely distorting the Raman excitation profiles of the heme modes, which are well explained by a Kramers–Kronig transform analysis that assumes coupling to only a single electronic state (Bangcharoenpaurpong et al., 1984).

Finally, when the line shapes of Mb and Mb* are compared at 10 K, we find a distinct broadening ($\sim$10%) of the Mb* species in both the Soret band and band III. The effect observed in Mb is opposite to that reported by Chavez et al. (1990) for hemoglobin A. One explanation for this difference involves the subunit heterogeneity in the band III line positions of Hb. The heterogeneity may be reduced in Hb*, accounting for the narrower line shape. We do not fully understand the opposite effect in Mb, but it may signal differences in the widths of the protein fluctuation spectrum of MbCO and Mb at the quenching temperature ($T_f \sim$ 185 K). Within the SRC model (Šrajer et al., 1988), this is accounted for by allowing the force constant associated with the protein coordinate (x) to depend upon the ligation state of the protein. Alternatively, it is possible that the coordinate distributions of the heme that develop in Mb*, after photolysis, are broader than for Mb.

Mb and Kinetic Hole-Burning Analysis.* The analysis of the static optical spectra associated with the low-temperature photoproduct, Mb*, is basically analogous to that of Mb. However, there are two additional observations associated with Mb* that allow explicit optical/kinetic models to be tested against experiment. These involve the red shift of the Mb* optical transitions with respect to Mb ($\Delta\tilde{\nu}^*_{ABS}$ = 137 cm^{-1}) and the kinetic hole burning (KHB) of the optical line shapes when the residual population of Mb* is monitored as a function of ligand rebinding. Experiments that quantitatively probe this latter effect in band III at low temperature [Ansari et al. (1985) as interpreted by Agmon (1988); Steinbach et al. (1991)] find a $\sim$45-cm^{-1} shift in the first moment (band position) after 90% of the rebinding from (Mb*, CO) to MbCO is completed.

The red shift of the Soret band and band III by the same amount, $\Delta\tilde{\nu}^*_{ABS} \sim$ 140 cm^{-1}, suggests that changes in a single coordinate affect both the Soret band and band III. We expect that the primary coordinate associated with the heme relaxation from Mb* to Mb involves heme doming, characterized by the iron out-of-plane displacement. In addition, we believe that this same coordinate is primarily responsible for the inhomogeneous distribution of barriers associated with the rebinding of (Mb*, CO) at low temperature (Šrajer et al., 1988). Thus, we assign the iron out-of-plane equilibrium position, a, as a "kinetic coordinate" (or, more properly, a kinetic control variable) involved both in determining the rebinding barrier height and the optical transition frequencies of Mb and Mb*.

In order to be more explicit we write

$$H(a) = H_0 + \alpha_H a + \beta_H a^2 \quad (1a)$$

$$\tilde{\nu}_0(a) = \tilde{\nu}_{00} + \alpha_\nu a + \beta_\nu a^2 \quad (1b)$$

where H is the barrier height associated with ligand binding and $\tilde{\nu}_0$ is the electronic transition frequency. Distributions in $\tilde{\nu}_0$, $P(\tilde{\nu}_0)$, lead to inhomogeneous broadening of the optical spectra. The kinetic control variable a has been allowed to couple to the energy spaces both linearly and quadratically in eq 1, although we will consider here only cases where one or the other is dominant (i.e., either α or β is set to zero). In cases of high symmetry [e.g., $\tilde{\nu}_0(a) \sim \tilde{\nu}_0(-a)$] or when linear restoring forces dominate [e.g., $H(a) \sim {}^1/_2 K a^2 \equiv \beta_H a^2$], the quadratic terms can be expected to play an important role. Moreover, after completion of the square in eq 1a, the coordinate axis can always be shifted (a $\rightarrow$ a′) so that α_H can be made to vanish (Šrajer et al., 1988). However, explicit use of the linear term α_H is unavoidable in other models (Agmon & Hopfield, 1983) where energetically significant low temperature relaxation of the heme is absent and the quadratic terms are dropped.

Scheme II

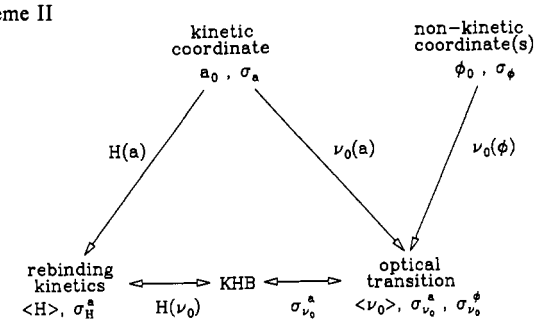

In addition to a, we will acknowledge the possibility that other degrees of freedom, ϕ, which are not significantly coupled to the kinetics, influence the optical transition frequencies. Thus, in general

$$\tilde{\nu}_0(a,\phi) = \tilde{\nu}_{00} + \alpha_{\tilde{\nu}} a + \beta_{\tilde{\nu}} a^2 + \gamma_{\tilde{\nu}}\phi + \delta_{\tilde{\nu}}\phi^2 \quad (2)$$

We set $\gamma_{\tilde{\nu}} = 0$ for the rest of the discussion to be consistent with the fact that quadratic coupling terms in the "nonkinetic coordinate" ϕ dominate the inhomogeneous broadening associated with the asymmetric Soret bands of Mb and Mb* (Šrajer et al., 1986). The use of ϕ as the variable for the nonkinetic coordinates emphasizes a previous suggestion that certain angular coordinates (histidine tilt and azimuthal orientation) may play a key role in the inhomogeneous broadening of the Soret band (Šrajer et al., 1986). An outline of the various sources of inhomogeneous broadening and their relationship to the rebinding kinetics and the KHB experiment is given in Scheme II.

It is also assumed that within an ensemble of totally photolyzed Mb* states at low temperature, there exists a distribution in the coordinate space that can be approximated by uncorrelated[3] Gaussian distributions:

$$P^*(a) = \frac{1}{\sigma_a\sqrt{2\pi}} e^{-(a-a_0^*)^2/2\sigma_a^2} \quad (3a)$$

$$P^*(\phi) = \frac{1}{\sigma_\phi\sqrt{2\pi}} e^{-(\phi-\phi_0^*)^2/2\sigma_\phi^2} \quad (3b)$$

Thus, we define the inhomogeneous optical width $\sigma_{\tilde{\nu}_0}$ as

$$2\sigma_{\tilde{\nu}_0} \equiv \tilde{\nu}_0(a_0^* + \sigma_a, \phi_0^* + \sigma_\phi) - \tilde{\nu}_0(a_0^* - \sigma_a, \phi_0^* - \sigma_\phi) \quad (4)$$

which leads to

$$\sigma_{\tilde{\nu}_0} = \alpha_{\tilde{\nu}}\sigma_a + 2\beta_{\tilde{\nu}} a_0^* \sigma_a + 2\delta_{\tilde{\nu}}\phi_0^*\sigma_\phi \quad (5)$$

and

$$\sigma_{\tilde{\nu}_0}^a \equiv \alpha_{\tilde{\nu}}\sigma_a + 2\beta_{\tilde{\nu}} a_0^*\sigma_a \quad (6a)$$

$$\sigma_{\tilde{\nu}_0}^\phi \equiv 2\delta_{\tilde{\nu}}\phi_0^*\sigma_\phi. \quad (6b)$$

In anticipation of the KHB results, we note that the distribution associated with the kinetic control variable $P^*(a)$ becomes time dependent as the ensemble begins to rebind CO and evolve from Mb* to MbCO. Thus, at time t after rebinding commences

$$P^*(a,t) = P^*(a)e^{-k(a)t} \quad (7)$$

where $k(a)$ is given by the usual Arrhenius expression

$$k(a) = k_0 e^{-H(a)/k_B T} \quad (8)$$

with barrier height $H(a)$ given by eq 1a. Note that a still more general treatment is needed when $T > 180$ K in order to account for the evolution of a_0^* toward the full out-of-plane displacement, $a_0 \sim 0.45$ Å [previously denoted $a_0^\dagger$ by Šrajer et al. (1988)]. Since we consider KHB only at temperatures below 60 K, and kinetics below 160 K, a_0^* is taken as a constant for the present work.

The full optical absorption lineshape $I(\tilde{\nu},t)$ is generated by a convolution of the coordinate distributions with the homogeneous line shape, $I_h[\tilde{\nu} - \tilde{\nu}_0(a,\phi)]$, so that

$$I(\tilde{\nu},t) = \int P^*(a,t)P^*(\phi)I_h[\tilde{\nu} - \tilde{\nu}_0(a,\phi)]\, d\phi\, da. \quad (9)$$

The homogeneous line-shape function is most easily generated with a time correlation formalism (Chan & Page, 1984) that has been applied previously to heme protein systems (Šrajer et al., 1986; Schomacker & Champion, 1986). The total line-shape function $I(\tilde{\nu},t)$ is proportional to the molecular absorption cross section $\sigma_A(\tilde{\nu})$ divided by the photon frequency $\tilde{\nu}$. The zeroth moment $M_0(t)$ and the higher moments are defined by

$$M_0(t) = \int I(\tilde{\nu},t)\, d\tilde{\nu} = \int P^*(a)e^{-k(a)t}\, da \quad (10)$$

$$M_1(t) = \frac{1}{M_0(t)}\int \tilde{\nu} I(\tilde{\nu},t)\, d\tilde{\nu} \quad (11)$$

$$M_2(t) = \frac{1}{M_0(t)}\int \tilde{\nu}^2 I(\tilde{\nu},t)\, d\tilde{\nu} - M_1^2(t) \quad (12)$$

where it can be seen from eq 10 that $M_0(t) \equiv N(t)$, the fraction of population remaining in the Mb* state at time t after the rebinding commences. The shift in the line position (first moment) with time, $\Delta M_1(t) = M_1(t) - M_1(0)$, is the primary observable in the KHB experiment, although changes in the line width with time, as characterized by $\Delta\sqrt{M_2(t)} = \sqrt{M_2(t)} - \sqrt{M_2(0)}$, may also be observable. Often, the actual time dependence of these quantities is not measured (Campbell et al., 1987; Chavez et al., 1990). Rather, the changes ΔM_1 and, in principle, $\Delta\sqrt{M_2}$ are monitored as a function of M_0.

In order to analyze the KHB experiment quantitatively, we derive some closed form expressions for the moments given by eqs 10–12. In Appendix A we consider a single control variable coupled linearly to both the optical frequency ($\beta_{\tilde{\nu}} = 0$) and barrier height ($\beta_H = 0$). We show that the shift in M_1 as a function of M_0 is indeed "universal" under certain well-defined circumstances. There have been previous qualitative discussions of this issue (Agmon, 1988) and some disagreement [Steinbach et al. (1991)]. The quantitative analysis given in Appendix A should help to clarify these issues. Of major importance is the result that within the "universal" regime that seems to apply for Mb* (Agmon, 1988) there is no quantitative information concerning the coupling (α_H and/or β_H) between the kinetic coordinate and the barrier height when ΔM_1 is measured as a function of M_0. In Appendix A we find that

$$\Delta M_1(0.1M_0) \sim 1.77\sigma_{\tilde{\nu}_0}^a \quad (13)$$

so that the shift in M_1 after 90% of the sample has rebound can be used *only* to determine the inhomogeneous optical width $\sigma_{\tilde{\nu}_0}^a$ due to the kinetic coordinate (see eq 6a).

For example, the observation of KHB in MbCO (Ormos et al., 1990) can be interpreted as evidence that the Fe–CO geometry is coupled to both the rebinding barrier and the MbCO Soret band. However, such measurements do not carry information about the relative importance of the Fe–CO coordinate in distributing the barrier heights, since that depends on both the width of the coordinate distribution and the

[3] If the coordinates are assumed to be correlated, one of them can always be eliminated from the analysis.

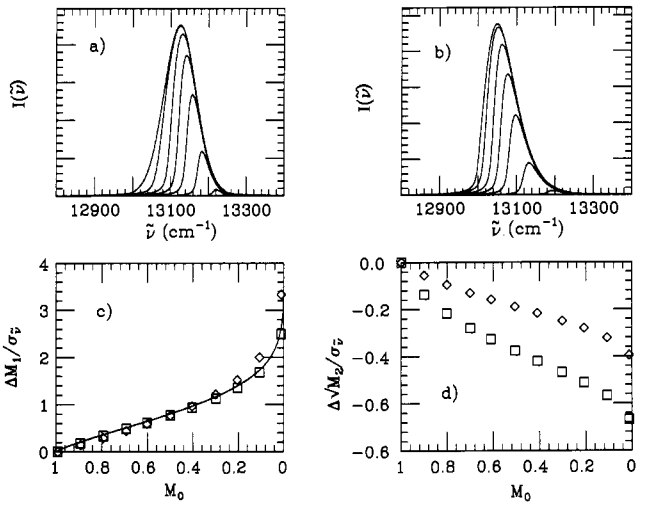

FIGURE 7: Simulations of the kinetic hole-burning experiment for an inhomogeneous absorption band ($\sigma_{\tilde{\nu}_0} = 40$ cm^{-1}, $\Gamma/2 = 5$ cm^{-1}, $\tilde{\nu}_{00} = 13\,000$ cm^{-1}). A linear relation for $\tilde{\nu}_0(a)$, with $\alpha_{\tilde{\nu}} = 500$ cm^{-1}/Å, is used in panel a, leading to a Gaussian line shape for the absorption band, while a quadratic relation for $\tilde{\nu}_0(a)$, with $\beta_{\tilde{\nu}} = 1000$ cm^{-1}/Å^2, is used in panel b, leading to an asymmetric line shape. In both panels a and b, the residual line shape is shown after 0, 10, 30, 50, 70, 90, and 99% of ligand recombination. A quadratic relation between the kinetic coordinate and the rebinding barrier, H, is used for both cases (with parameters that correspond to $a_0^* = 0.25$ Å, $\sigma_a = 0.08$ Å, $\beta_H = 78$ kJ/mol Å^2, $H_0 = 7$ kJ/mol, and $k_0 = 3 \times 10^9$ s^{-1}). The lower part of the figure shows the shift of the first moment, ΔM_1 (c) and square root of the second moment $\Delta\sqrt{M_2}$ (d), both normalized to $\sigma_{\tilde{\nu}_0}$, as the rebinding progresses. The squares present the effect of KHB using the lineshapes in panel a and the diamonds the results for the line shapes in panel b. The solid line in panel c corresponds to the closed form expressions derived in Appendix A, assuming both $\tilde{\nu}_0$ and H to be linear in a. Changes in the homogeneous damping factor Γ, or inclusion of vibrational broadening, do not affect the shift of the first moment shown in panel c. However, the reduction of the full width of the line shapes during KHB is suppressed as these other contributions to the line shape are increased (Šrajer, 1991).

magnitude of the coupling coefficients (α_H and/or β_H). In order to obtain quantitative information concerning the coupling between the coordinates and the barrier height, the time and temperature dependence of $M_1(t)$ and $M_0(t)$ must be measured in the KHB experiment.

In Figure 7 we display some examples of simulations involving quadratic as well as linear coupling between the coordinate and optical frequency. Both examples shown in the figure utilize the simple harmonic (quadratic) picture for the rebinding barrier height presented previously (Šrajer et al., 1988). In panel a we take the optical coupling to be linear ($\beta_{\tilde{\nu}} = 0$) and observe the expected Gaussian line shapes. The change in the line position is quite obvious as the rebinding proceeds and the shift of M_1, normalized to $\sigma_{\tilde{\nu}_0}{}^a$, is plotted vs M_0 as the open squares in panel c. A similar effect is noted in panel b when the inhomogeneous optical coupling is quadratic ($\alpha_{\tilde{\nu}} = 0$) and the line shape is asymmetric. The normalized first moment shifts for this case are plotted as open diamonds in panel c. The solid line is the result for $\Delta M_1(M_0)$ derived in Appendix A. For completeness, we also plot the changes in the linewidth $\Delta\sqrt{M_2}$, also normalized to $\sigma_{\tilde{\nu}_0}{}^a$, for the two examples in panel d. Here we have set the underlying Lorentzian components to zero, since they have divergent second moments.

Analysis of the KHB measurements in band III yields $\Delta M_1(0.1M_0) \sim 45$ cm^{-1} (Agmon, 1988; Steinbach et al., 1991), so we use Figure 7c and eqs 13 and 6a to approximate

$$\sigma_{\tilde{\nu}_0}{}^a = \alpha_{\tilde{\nu}}\sigma_a + 2\beta_{\tilde{\nu}}a_0^*\sigma_a \sim 25 \text{ cm}^{-1} \quad (14)$$

which is almost exactly the same magnitude as the total inhomogeneous broadening observed in band III. This suggests that the kinetic coordinate is the only active coordinate involved in the inhomogeneous broadening of band III (i.e., $\delta_{\tilde{\nu}} \sim 0$ for band III). In the Soret band, the quantity $\delta_{\tilde{\nu}}$ must be nonzero to account for an inhomogeneous width that is much larger than the kinetic inhomogeneity. Such a situation might arise, for example, if the coordinate ϕ primarily perturbs the extended π^* orbitals of the porphyrin.

Since only a single coordinate is involved for band III, we find

$$\Delta\tilde{\nu}_{ABS}^* = \tilde{\nu}_0(a_0) - \tilde{\nu}_0(a_0^*) = \alpha_{\tilde{\nu}}(a_0 - a_0^*) + \beta_{\tilde{\nu}}(a_0^2 - a_0^{*2}) \quad (15)$$

so that the coupling coefficient associated with either the linear ($\beta_{\tilde{\nu}} = 0$) or the quadratic ($\alpha_{\tilde{\nu}} = 0$) model can be found if a_0 and a_0^* are known.[4] Thus, if we take $a_0 = 0.45$ Å, we can find a_0^* from the KHB experiment (eq 14) and the low-temperature rebinding kinetics by using

$$a_0^{*\prime}/\sigma_a \sim 3.1 \quad (16)$$

which is uniquely determined from the fits to the low-temperature kinetics by using the SRC model [see eq 15 and Table II in Šrajer et al. (1986)].

The prime on the parameter a_0^* denotes that it is extracted from the fits to the low-temperature kinetics and appears in eq 16 to accommodate the possibility of significant contributions from the "static" protein coordinate (x) that arise when the low-temperature heme relaxation is incomplete. As mentioned above [see also footnote 21 in Šrajer et al. (1988)], eq 1a can always be transformed so that $\alpha_H = 0$, even when the static protein coordinate (x) is included in the analysis. However, in this most general case the value for $a_0^{*\prime}$, as recovered from the fit to the low-temperature kinetics, is shifted from the true value of a_0^* so that

$$a_0^{*\prime} = a_0^* + \frac{k_B T_f (a_0 - a_0^*)}{3K\sigma_a{}^2} \quad (17)$$

When the low-temperature relaxation of the heme is significant, $a_0^* \gtrsim 0.35$ Å, we find that $a_0^{*\prime} \sim a_0^*$ and the static protein-dependent terms that dominate the low-temperature analysis of Agmon and Hopfield (1983) can be ignored [cf. eq 36 of Šrajer et al. 1988)]. On the other hand, if the heme relaxation at low temperature is incomplete, and $a_0^* \lesssim 0.35$ Å, the static protein-dependent terms need to be included via eq 17. In the limit that there is no low-temperature heme relaxation and the coupling between the protein and heme coordinates goes to zero, the SRC model reduces to the results of Agmon and Hopfield (see Appendix B).

Since the product $K\sigma_a{}^2 \sim 1$ kJ/mol is also an invariant in the fits to the low-temperature kinetics, the fitting parameter $a_0^{*\prime}$ can be eliminated in eqs 16 and 17 so that eqs 14–17 form a closed set with three unknowns: a_0^*, σ_a, and either $\alpha_{\tilde{\nu}}$ or $\beta_{\tilde{\nu}}$ for the linear or quadratic model of inhomogeneous optical broadening, respectively.

Table II presents the solutions to these equations for the two models of inhomogeneous broadening (cases I and II). In addition, the linear model of Agmon and Hopfield (1983) with no heme relaxation (case III) and case IV, involving complete heme relaxation ($a_0^* = a_0 = 0.45$ Å), are included for comparison. Note that complete heme relaxation at low tem-

[4] If we assume that the equal red shift, $\Delta\tilde{\nu}_{ABS}^* \sim 140$ cm^{-1}, of the Soret band and band III is not a coincidence, the coupling coefficients for the kinetic coordinate in both transitions must be the same. In this case, eq 15 also holds for the Soret band, if $\phi_0 = \phi_0^*$.

Table III: Effect of Heme Relaxation on Optical and Kinetic Observables[a]

a_0^*	σ_a	β_H	β_ν	$\Delta\tilde{\nu}^*_{abs}$	$\sigma_{\tilde{\nu}_0}{}^a$	E_A
			1713	137[b]	156	
0.35	0.13	31				11.9
			275	22	25[b]	
			977	137[b]	56	
0.25	0.11	40				14.6
			435	61	25[b]	

[a] a_0, σ_a, β_H, β_ν, and E_A have the same units as in Table II; $\Delta\tilde{\nu}^*_{ABS}$ and $\sigma_{\tilde{\nu}_0}{}^a$ are in cm^{-1}. [b] Experimentally observed value.

perature is incompatible with the observation of the shifts in the optical transition frequencies, since it predicts $\Delta\tilde{\nu}^*_{ABS} = 0$. Another major difference between the various cases occurs in the magnitude of the predicted high-temperature Arrhenius barrier height, E_A, obtained by averaging over the high-temperature distributions of a (or x). Appendix B presents some general expressions within the SRC model, useful for extrapolation of the low-temperature barrier height distribution to the high-temperature Arrhenius limit.

The cases that involve very little heme relaxation at low temperature will always lead to significantly larger barrier heights (~30 kJ/mol) than those that allow for at least some heme relaxation after the ligand is flashed off at low temperature. This can be seen most easily from the fact that the peak of the low-temperature barrier distribution, E_p(<180 K) $\sim {}^1/_2 K a_0^{*2}$ (which is found near 10 kJ/mol for MbCO), will be closer to the peak of the high-temperature distribution, E_p(290 K) $\sim {}^1/_2 K a_0^2$, as a_0^* approaches a_0. The increase in a_0, as more low-temperature relaxation is allowed, results in smaller values for K and E_p(290 K), thus reducing the Arrhenius barrier, E_A [see Šrajer et al. (1988) for more details].

It should also be noted that the linear model ($\beta_H = 0$) employed by Agmon and Hopfield (1983) cannot be valid if energetically significant heme relaxation, subsequent to photolysis, is allowed at low temperature. This is due to the fact that the relaxation of the heme coordinates at low temperature leads to quadratic terms in the rebinding barrier, *even* when the force constants associated with the bound and deoxy states are taken to be equal.

There are a variety of experiments involving resonance Raman (Rousseau & Argade, 1986), EXAFS (Powers et al., 1987), and infrared (Fiamingo & Alben, 1985) that indicate that a_0^* is nonzero in the low-temperature photoproduct. On the basis of these independent observations, we suggest that the partial relaxation model, utilizing quadratic coupling for the inhomogeneous distribution of optical frequencies (case I), is most compatible with the overall body of experimental evidence. The value for $a_0^* = 0.16$ Å, obtained in this case, is smaller than previously suggested (Šrajer et al., 1988) and predicts an Arrhenius barrier height of 18 kJ/mol.

As an example of the sensitivity of the optical measurements and Arrhenius barrier to a_0^*, we display in Table III the values of $\sigma_{\tilde{\nu}_0}{}^a$, $\Delta\tilde{\nu}^*_{ABS}$, and E_A that are predicted when other values for a_0^* are assumed. We have presented cases where either $\Delta\tilde{\nu}^*_{ABS}$ or $\sigma_{\tilde{\nu}_0}{}^a$ are set equal to their experimental values. Other optical (β_ν) and kinetic parameters (β_H, σ_a), associated with the different cases, are also summarized in Tables II and III. Notice that as a_0^* approaches 0.25 Å the optical observations are reproduced to within a factor of 2.

If we allow additional nonkinetic degrees of freedom to couple to band III, they must be narrowly distributed, and, if their mean position shifts between Mb and Mb*, the major effect is to reduce the amount of $\Delta\tilde{\nu}^*_{ABS}$ associated with the kinetic coordinate in eq 15. This leads to larger values of a_0^* when eqs 14–17 are solved. For example, the case with $a_0^* = 0.25$ Å in Table III leads to $\Delta\tilde{\nu}^*_{ABS} = 61$ cm^{-1} and is consistent with significant coupling to a narrowly distributed nonkinetic degree of freedom in band III. Thus, within the constraints of the SRC model and the experimental observations, we find $a_0^* = 0.2 \pm 0.05$ Å and predict $E_A = 16 \pm 2$ kJ/mol for the high-temperature barrier at the heme.

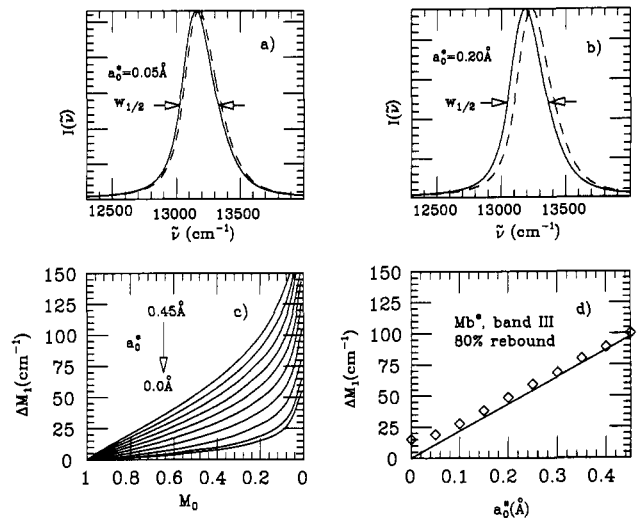

FIGURE 8: Kinetic hole burning of the Mb* band III line shape, at 80 K, after 80% ligand recombination (dashed curves) is simulated for two values of a_0^*: 0.05 Å (a) and 0.20 Å (b), for the case of quadratic optical coupling (solid curves, $t = 0$). The parameters used to simulate the line shape (no background added) are the same as for Figure 3, with the inhomogeneous broadening parameters from Table II (case I). The FWHM of the line shapes, $w_{1/2}$, are found to be 309 cm^{-1} (a) and 338 cm^{-1} (b), indicating how other sources of broadening can make the KHB width changes difficult to detect, even though the shifts are readily apparent. The first moment shifts, as rebinding progresses, are shown in panel c for values of a_0^* between 0 and 0.45 Å (in steps of 0.05 Å). The first moment shifts at 80% recombination are shown in panel d as a function of the iron displacement a_0^* (diamonds). The solid line corresponds to the prediction of the approximate eq 18. Note from panel c that the shifts are highly nonlinear between 80% and 100% recombination in both the linear and quadratic models (see also Figure 7c). Band III in Hb is monitored after 87% recombination in the T-state and after only 80% in the R-state (Chavez et al., 1990). This may also account partially for the difference in the magnitude of the observed KHB shifts in the two states.

Studies of Band III in Hemoglobin. A previous study of HbA and the Fe–Mn hybrids by Chavez et al. (1990) has demonstrated the sensitivity of the band III position to subunit and quaternary structure. Moreover, it demonstrated significantly enhanced KHB of the T-state structures when compared to the R-state. However, as we have shown in Appendix A and eq 13, the measurement of the KHB shifts of Mb* are insensitive to the coupling (i.e., α_H or β_H) between the coordinates and the barrier height. As a result, caution should be exercised in the interpretation of the KHB results if information about α_H or β_H is to be inferred.

When the overall band width is dominated by homogeneous, vibrational, or nonkinetic inhomogeneous broadening, changes in the observed width (arising from the kinetic inhomogeneous broadening) may be difficult to detect and only the shift will be seen (e.g., Figure 8a,b). The situation in Hb is more complicated, due to the subunit heterogeneity, which can mask line-width changes altogether.

A simple explanation for the enhanced T-state KHB shifts arises naturally within the quadratic model for inhomogeneous broadening of the optical transition. In Figure 8 we display the results of line-shape simulations that monitor the mag-

nitude of the KHB shift as a function of a_0^*. We find that the shift in position, $\Delta M_1(M_0)$, after 80% of the ligands have recombined, depends sensitively on the magnitude of a_0^*. This is due to the fact that the shift is proportional to the inhomogeneous broadening associated with the kinetic coordinate. In the quadratic model, the kinetic inhomogeneous broadening scales linearly with a_0^* when $a_0^* \gtrsim \sigma_a$ (eq 6a with $\alpha_{\tilde{\nu}} = 0$). For smaller values of a_0^*, the trend is preserved, but the relation is nonlinear and computer simulations are needed. Equations A8 and 6a (with $\alpha_{\tilde{\nu}} = 0$) can be combined to give

$$\Delta M_1(0.2M_0) = 2.78\beta_{\tilde{\nu}} a_0^* \sigma_a \qquad (18)$$

which approximates the relationship between the underlying kinetic coordinate distribution and the magnitude of the KHB shift after 80% ligand recombination. The solid line in Figure 8d compares eq 18 with the exact simulation.

Assuming that the T structures allow the iron to relax further out of plane in the low temperature photoproduct than the R structures, leads directly to the observations of Chavez et al. (1990). Moreover, if $\tilde{\nu}_{00}$ and $\beta_{\tilde{\nu}}$ are taken to be independent of subunit and quaternary structure, we can use eq 1b and the observed (Chavez et al., 1990) band III positions of the photoproducts to predict

$$a_0^*(\beta R) < a_0^*(\alpha R) \sim a_0^*(\beta T) < a_0^*(\alpha T)$$

which is also consistent with the analysis of enhanced T-state KHB and the result expected from the high-temperature X-ray structures (Perutz et al., 1987). The $\sim$52-cm^{-1} blue shift of band III in Hb compared to Mb (Cordone et al., 1986, Cupane et al., 1988) follows directly from eq 1b [$\Delta\tilde{\nu}_{abs} = \beta_{\tilde{\nu}}[a_0^2(\text{Hb}) - a_0^2(\text{Mb})] = 55$ cm^{-1}] when the larger iron displacements from the heme plane[5] found in Hb [a_0(Mb) = 0.47 Å and a_0(Hb) = 0.54 Å, Perutz et al. (1987)] are used with $\beta_{\tilde{\nu}} = 781$ cm^{-1} (Table II).

Finally, we point out that the correlation of the $\tilde{\nu}_{\text{Fe-His}}$ Raman mode with the out-of-plane displacement and position of band III (Sassaroli & Rousseau, 1987; Chavez et al., 1990) is not inconsistent with the above analysis. However, it must be understood that the $\tilde{\nu}_{\text{Fe-His}}$ Raman frequency is only an indirect measure of the out-of-plane displacement and probably does not vary in a linear fashion with the displacement. It is clearly possible for the equilibrium position of a coordinate to shift without altering the frequency of the mode (this is known as linear coupling in optical theory and is often invoked as a "standard assumption"). It seems likely that, when the iron displacement in the photoproduct is small, the histidine does not need to tilt and the $\tilde{\nu}_{\text{Fe-His}}$ mode is relatively insensitive to the displacement. Since small (but differing) displacements are likely to be associated with the α and β chains of the R-state photoproduct, the observation of identical $\tilde{\nu}_{\text{Fe-His}}$ frequencies and differing band III positions for these subunits (Chavez et al., 1990) can be explained without the need for other coordinates affecting the barrier height. On the other hand, when the displacements become larger at higher temperature, at longer times, or in the T-states, the histidine is forced to tilt, causing the Fe–His bond to be strained and its frequency to be lowered.

Conclusions

In this study the optical line shapes associated with Mb, Mb*, and MbCO have been analyzed under various conditions of temperature and pH. We find that a low-frequency subspace associated with torsions of the bound CO molecule strongly influences the thermal properties of the Soret band in MbCO. This effect is more pronounced at low pH when the distal heme pocket is thought to be in a more "open" conformation and less pronounced in MbO_2 (pH 7) where the ligand is restrained by hydrogen bonding. The spectra associated with Mb and Mb* are found to be quite similar except for a shift in position by $\sim$140 cm^{-1}. The asymmetric Soret bands of these states have a significant component of inhomogeneous broadening, induced by a "nonkinetic" coordinate. The band at 760 nm (band III) is also asymmetric, but its temperature dependence indicates that the asymmetry is mainly induced by coupling to low-frequency vibrational modes, possibly involving heme doming. The intensity of this band as a function of temperature is consistent with numerous low lying electron states in the deoxy-Mb system. The lineshape analysis finds that only $\sim$25 cm^{-1} of the total width of band III is due to "static" inhomogeneous broadening. We suggest that this inhomogeneity can be attributed to an underlying kinetic control variable that is associated with the iron out-of-plane displacement and accounts for the observation of kinetic hole burning. The quantitative analysis of the KHB, along with the shifts in the optical line positions that occur at 185 K, are consistent with the low-temperature kinetics if a quadratic heme relaxation (SRC) model for the ligand-binding reaction is employed. A quadratic model for the optical coupling is also consistent with a significant iron out-of-plane displacement in Mb* ($\sim$0.2 Å) and with the observation of enhanced KHB in the T-states of Hb. Linear models that do not acknowledge the low-temperature heme relaxation can also account for the low-temperature observables but differ significantly in their prediction of the high-temperature Arrhenius barrier. It remains possible that the heme relaxation is a temperature-dependent process that leads to some evolution of the barrier height distribution, even at temperatures below 160 K. However, a major structural transition of the heme is observed to take place at 185 K in parallel with a protein transition that allows ligand escape to the solvent.

Acknowledgments

We thank Dr. Tim Sage for helpful discussions and Prof. Hans Frauenfelder for supplying a manuscript prior to publication.

Appendix A

From eqs 1 and 7–9 in the text, the time evolution of the absorption line shape can be written as

$$I(\tilde{\nu},t) = I(\tilde{\nu},0)e^{-k(\tilde{\nu})t} \qquad (A1)$$

where

$$k = k_0 \exp(-H/k_B T) \qquad (A2)$$

and

$$H = H_0 + \frac{\alpha_H}{\alpha_{\tilde{\nu}}}(\tilde{\nu} - \tilde{\nu}_{00}) \qquad (A3)$$

if only the linear terms in eq 1 are retained and $I_h = \delta(\tilde{\nu} - \tilde{\nu}_0)$. The time-dependent exponential that enters eq A1 can be written as

$$\exp(-k_0 t e^{-H/k_B T}) = \exp(-e^{(\tilde{\nu}'-\tilde{\nu})/\gamma}) \qquad (A4)$$

where

$$\tilde{\nu}' = \frac{\alpha_{\tilde{\nu}}}{\alpha_H}(k_B T \ln k_0 t - H_0) + \tilde{\nu}_{00} \qquad (A5)$$

and

[5] Mean heme plane of porphyrin N's and C's, including the first atom of each side chain.

$$\gamma = \frac{\alpha_{\tilde{\nu}}}{\alpha_H} k_B T \tag{A6}$$

The exponential in eq A4 can be approximated by a step function at $\tilde{\nu}'$ in these calculations, so long as $e\gamma < \sigma_{\tilde{\nu}}$. In this case we find

$$M_0(t) = \int_{\tilde{\nu}'(t)}^{\infty} I(\tilde{\nu},0)\, d\tilde{\nu} \tag{A7a}$$

$$M_1(t) = \frac{1}{M_0(t)} \int_{\tilde{\nu}'(t)}^{\infty} \tilde{\nu} I(\tilde{\nu},0)\, d\tilde{\nu} \tag{A7b}$$

This leads to

$$M_0(t) = (1/2)[1 - \mathrm{erf}(y)] \tag{A8a}$$

$$\Delta M_1(t) = \frac{\sigma_{\tilde{\nu}}}{M_0(t)\sqrt{2\pi}} e^{-y^2} \tag{A8b}$$

where

$$y = \frac{\tilde{\nu}'(t) - \tilde{\nu}_{00} - \alpha_{\tilde{\nu}} a_0}{\sqrt{2}\sigma_{\tilde{\nu}}}. \tag{A9}$$

We can see from eq A8 that, if one monitors ΔM_1 vs M_0, the information about the parameters in eq A5 is concealed by the parametric dependence of ΔM_1 and M_0 on y. The first moment shift as a function of M_0 can only be used to find $\sigma_{\tilde{\nu}} = \alpha_{\tilde{\nu}}\sigma_a$. For example, we find that at 90% of recombination

$$\Delta M_1 = 1.77\sigma_{\tilde{\nu}} \tag{A10}$$

We also find that for the case of kinetic hole burning of the 760-nm band of Mb*, the above approximation holds, since we arrive at the same value of $\sigma_{\tilde{\nu}}$ by using eq A10 as extracted by Agmon (1988) using a more complex fitting procedure. As shown in Figure 7 and Šrajer (1991), similar results are obtained if the barrier height and optical frequencies are assumed to have a quadratic coordinate dependence so that $H = H_0 + (\beta_H/\beta_{\tilde{\nu}})(\tilde{\nu} - \tilde{\nu}_{00})$.

Appendix B

Within the SRC model, the Arrhenius barrier height can be obtained by averaging k_{BA} over the underlying coordinate space. This average can be carried out by using either the generalized protein coordinate (x) or the iron out-of-plane equilibrium position (a) since they are related by

$$a(x) = a_0^* + \alpha(x - x_0) \tag{B1}$$

The probability of finding the deoxy-Mb at x is given by

$$P(x) = \sqrt{\frac{f}{2\pi k_B T}} \exp(-fx^2/2k_B T) \tag{B2}$$

where the protein is free to diffuse at high temperature and f is a force constant that holds the the protein in its equilibrium conformation. The Arrhenius barrier height E_A can be expressed in terms of the peak of the low-temperature barrier height distribution E_p so that

$$E_A = E_p + \Delta E \tag{B3}$$

where

$$E_p = \Delta'_v/3 + (1/2)Ka_0^{*\prime 2} \tag{B4}$$

and

$$\Delta E = (1/3)fx_0^2 - (1/2)K\alpha x_0 a_0 - \frac{(K\alpha a_0 - (1/3)fx_0)^2}{2(f + K\alpha^2)} \tag{B5}$$

The quantities Δ'_v and $a_0^{*\prime}$ are fitting parameters involving the potential energies of both the protein and heme coordinates, K is the iron–porphyrin force constant, and x_0 is the protein equilibrium position of MbCO [see footnote 21 of Šrajer et al. (1988) for more details]. The mean iron out-of-plane displacement of deoxy-Mb at high temperature follows from B1 and B2 and is given by

$$a_0 = a_0^* - \alpha x_0 \tag{B6}$$

In the full low temperature relaxation limit ($x_0 = 0$, $a_0^* = a_0$) we recover

$$E_A = \Delta_v/3 + (1/2)Ka_0^{*2}(1 + K\alpha^2/f)^{-1} \tag{B7}$$

which is analogous to eq 33b in Šrajer et al. (1988), since $\alpha^2/f = \sigma_a^2/k_B T_f$ from eqs B1 and B2. Note that eq B7 predicts that E_A is *less* than E_p when full relaxation is allowed. In the limit of no relaxation at low temperature ($a_0^* = 0$) we find

$$\Delta E = (1/3)fx_0^2 + (1/2)K(\alpha x_0)^2 - \frac{(K\alpha^2 x_0 + (1/3)fx_0)^2}{2(f + K\alpha^2)} \tag{B8a}$$

$$E_p = \Delta_v/3 - fx_0^2/6 \tag{B8b}$$

so that the Agmon–Hopfield result emerges when the protein and heme are decoupled ($\alpha = 0$ and $\sigma_a = 0$). Note the error in eq 14 of Agmon and Hopfield (1983), which should read $E_A = \Delta/3 + fx_0^2/9$.

Registry No. Heme, 14875-96-8.

References

Agmon, N. (1988) *Biochemistry 27*, 3507.

Agmon, N., & Hopfield, J. J. (1983) *J. Chem. Phys. 79*, 2042.

Ansari, A., Berendzen, J., Bowne, S., Frauenfelder, H., Iben, I., Sauke, T., Shyamsunder, E., & Young, R. (1985) *Proc. Natl. Acad. Sci. U.S.A. 82*, 5000.

Ansari, A., Berendzen, J., Braunstein, D., Cowen, B. R., Frauenfelder, H., Hong, M. K., Iben, I. E. T., Johnson, J. B., Ormos, P., Sauke, T. B., Scholl, R., Schulte, A., Steinbach, P. J., Vittitow, J., & Young, R. D. (1987) *Biophys. Chem. 26*, 337.

Austin, R. H., Beeson, K. W., Eisenstein, L., Frauenfelder, H., & Gunsalus, I. C. (1975) *Biochemistry 14*, 5355.

Bangcharoenpaurpong, O., Schomacker, K. T., & Champion, P. M. (1984) *J. Am. Chem. Soc. 106*, 5688.

Bevington, P. R. (1969) *Data Reduction and Error Analysis for the Physical Sciences*, McGraw-Hill, Inc., New York.

Campbell, B., Chance, M., & Friedman, J. (1987) *Science 238*, 373.

Chan, C., & Page, J. B. (1984) *Chem. Phys. Lett. 104*, 609.

Chavez, M., Courtney, H., Chance, M., Kiula, D., Nocek, J., Hoffman, B., Friedman, J., & Ondrias, M. (1990) *Biochemistry 29*, 4844.

Collins, D., Champion, P. M., & Fitchen, D. B. (1976) *Chem. Phys. Lett. 40*, 416.

Cordone, L., Cupane, A., Leone, M., & Vitrano, E. (1986) *Biophys. Chem. 24*, 259.

Cupane A., Leone, M., Vitrano, E., & Cordone, L. (1988) *Biopolymers 27*, 1977.

Fiamingo, F. G., & Alben, J. O. (1985) *Biochemistry 24*, 7964.

Hong, M., Braunstein, D., Cowen, B., Frauenfelder, H., Iben, I., Mourant, J., Ormos, P., Scholl, R., Schulte, A., Steinbach, P., Xie, A., & Young, R. (1990) *Biophys. J. 58*, 429.

Huynh, B., Papaefthymiou, G., Yen, C., Groves, J. & Wu, C. S. (1974) *J. Chem. Phys. 61*, 3750.

Iizuka, T., Yamamoto, H., Kotani, M., & Yonetani, T. (1974) *Biochim. Biophys. Acta 351*, 182.

Kent, T., Spartalian, K., & Lang, G. (1979) *J. Chem. Phys. 71*, 4899.
Kuriyan, J., Wilz, S., Karplus, M., & Petsko, G. (1986) *J. Mol. Biol. 192*, 133.
Moore, J., Hansen, P., & Hochstrasser, R. (1988) *Proc. Natl. Acad. Sci. U.S.A. 85*, 5062.
Morikis, D., Champion, P. M., Springer, B. A., & Sligar, S. G. (1989) *Biochemistry 28*, 4791.
Morikis, D., Li, P., Bangcharoenpaurpong, O., Sage, J. T., & Champion, P. M. (1991) *J. Phys. Chem. 95*, 3391.
Ormos, P., Braunstein, D., Frauenfelder, H., Hong, M., Lin, S., Sauke, T., & Young, R. (1988) *Proc. Natl. Acad. Sci. U.S.A. 85*, 8492.
Ormos, P. Ansari, A., Braunstein, D., Cowen, B. R., Frauenfelder, H., Hong, M. K., Iben, I. E. T., Sauke, T. B., Steinbach, P. J., & Young, R. D. (1990) *Biophys. J. 57*, 191.
Perutz, M., Fermi, G., Luisi, B., Shaanan, B., & Liddington, R. C. (1987) *Acc. Chem. Res. 20*, 309.
Powers, L., Chance, B., Chance, M., Campbell, B., Friedman, J., Khalid, S., Kumar, C., Naqui, A., Reddy, K., & Zhou, Y. (1987) *Biochemistry 26*, 4785.
Rousseau, D., & Argade, P. (1986) *Proc. Natl. Acad. Sci. U.S.A. 83*, 1310.
Sassaroli, M., & Rousseau, D. (1987) *Biochemistry 26*, 3092.
Schomacker, K., & Champion, P. M. (1986) *J. Chem. Phys. 84*, 5314.
Shimada, H., & Caughy, W. (1982) *J. Biol. Chem. 257*, 11893.
Šrajer, V. (1991) Ph.D. Thesis, Northeastern University.
Šrajer, V., Schomacker, K. T., & Champion, P. M. (1986) *Phys. Rev. Lett. 57*, 1267.
Šrajer, V., Reinisch, L., & Champion, P. M. (1988) *J. Am. Chem. Soc. 110*, 6656.
Šrajer, V., Reinisch, L., & Champion, P. M. (1991) *Biochemistry 30*, 4886-4895.
Steinbach, P., Ansari, A., Berendzen, J., Braunstein, D., Chu, K., Cowen, B., Ehrenstein, D., Frauenfelder, H., Johnson, J., Lamb, D., Luck, S., Mourant, J., Nienhaus, G., Ormos, P., Philipp, R., Scholl, R., Xie, A., & Young, R. (1991) *Biochemistry 30*, 3988-4001.
Warshel, A. (1977) *Proc. Natl. Acad. Sci. U.S.A. 74*, 1789.
Young, R. D., & Bowne, S. F. (1984) *J. Chem. Phys. 81*, 3730.

Sequence-Specific ^{1}H NMR Assignments, Secondary Structure, and Location of the Calcium Binding Site in the First Epidermal Growth Factor Like Domain of Blood Coagulation Factor IX†

Linda H. Huang,‡ Hong Cheng,‡ Arthur Pardi,§ James P. Tam,∥ and William V. Sweeney*,‡

Department of Chemistry, Hunter College, 695 Park Avenue, New York, New York 10021, Department of Chemistry and Biochemistry, University of Colorado, Boulder, Colorado 80309-0215, and The Rockefeller University, 1230 York Avenue, New York, New York 10021

Received December 19, 1990; Revised Manuscript Received April 2, 1991

ABSTRACT: Factor IX is a blood clotting protein that contains three regions, including a γ-carboxyglutamic acid (Gla) domain, two tandemly connected epidermal growth factor like (EGF-like) domains, and a serine protease region. The protein exhibits a high-affinity calcium binding site in the first EGF-like domain, in addition to calcium binding in the Gla domain. The first EGF-like domain, factor IX (45-87), has been synthesized. Sequence-specific resonance assignment of the peptide has been made by using 2D NMR techniques, and its secondary structure has been determined. The protein is found to have two antiparallel β-sheets, and preliminary distance geometry calculations indicate that the protein has two domains, separated by Trp^{28}, with the overall structure being similar to that of EGF. An NMR investigation of the calcium-bound first EGF-like domain indicates the presence and location of a calcium binding site involving residues on both strands of one of the β-sheets as well as the N-terminal region of the peptide. These results suggest that calcium binding in the first EGF-like domain could induce long-range (possibly interdomain) conformational changes in factor IX, rather than causing structural alterations in the EGF-like domain itself.

Factor IX is a vitamin K dependent blood clotting protein important in the intrinsic clotting cascade. This protein has a domain structure consisting of an N-terminal γ-carboxyglutamic acid (Gla)[1] domain, two epidermal growth factor like (EGF-like) domains, and a C-terminal serine protease domain.

A wide range of blood clotting proteins contain tandem repeats of an epidermal growth factor like domain, including factor IX, factor X, factor XII, factor VII, protein S, and protein C (Furie & Furie, 1988). The function of these EGF-like domains is not understood. It has been shown that no EGF-receptor binding or mitogenic activity is present in a peptide consisting of only the first EGF-like domain of factor IX (Huang et al., 1989). However, calcium binding is required

† This research was supported by U.S. Public Health Service National Institutes of Health Grants HL41935 (J.P.T. and W.V.S.) and AI27026 (A.P.).

* Author to whom correspondence should be addressed.
‡ Hunter College.
§ University of Colorado.
∥ The Rockefeller University.

[1] Abbreviations: EGF, epidermal growth factor; TGF, tumor growth factor; Gla, γ-carboxyglutamic acid; 2D, two dimensional; NMR, nuclear magnetic resonance; COSY, two-dimensional correlation spectroscopy; DQF-COSY, two-dimensional double-quantum-filtered correlation spectroscopy; RELAY-COSY, two-dimensional relayed coherence-transfer spectroscopy; TOCSY, two-dimensional total correlation spectroscopy; TQ-COSY, triple-quantum coherence-transfer spectroscopy; t_1, evolution time; FID, free induction decay.

0006-2960/91/0430-7402$02.50/0